American Mineralogist, Volume 100, pages 588–597, 2015

P-V-T equation of state of $Ca_3Cr_2Si_3O_{12}$ uvarovite garnet by using a diamond-anvil cell and in-situ synchrotron X-ray diffraction

Dawei Fan[1,*], Jingui Xu[1,2], Maining Ma[2,3], Shuyi Wei[1,2], Bo Zhang[1,2], Jing Liu[4] and Hongsen Xie[1]

[1]Key Laboratory for High Temperature and High Pressure Study of the Earth's Interior, Institute of Geochemistry, Chinese Academy of Sciences, Guiyang 550002, China
[2]University of Chinese Academy of Sciences, Beijing 100049, China
[3]Key Laboratory of Computational Geodynamics, Chinese Academy of Sciences, Beijing 100049, China
[4]Beijing Synchrotron Radiation Facility, Institute of High Energy Physics, Chinese Academy of Sciences, Beijing 100049, China

Abstract

The pressure-volume-temperature (*P-V-T*) equation of state (EoS) of synthetic uvarovite has been measured at high temperatures up to 900 K and high pressures up to 16.20 GPa, by using in situ angle-dispersive X-ray diffraction and diamond-anvil cell. Analysis of room-temperature *P-V* data to a third-order Birch-Murnaghan EoS yielded: $V_0 = 1736.9 \pm 0.5$ Å^3, $K_0 = 162 \pm 2$ GPa, and $K_0' = 4.5 \pm 0.3$. With K_0' fixed to 4.0, we obtained: $V_0 = 1736.5 \pm 0.3$ Å^3 and $K_0 = 164 \pm 1$ GPa. Fitting of our *P-V-T* data by means of the high-temperature third-order Birch-Murnaghan equations of state, given the thermoelastic parameters: $V_0 = 1736.8 \pm 0.8$ Å^3, $K_0 = 162 \pm 3$ GPa, $K_0' = 4.3 \pm 0.4$, $(\partial K/\partial T)_P = -0.021 \pm 0.004$ GPa/K, and $\alpha_0 = (2.72 \pm 0.14)\times10^{-5}$ K^{-1}. We compared our elastic parameters to the results from the previous studies for uvarovite. From the comparison of these fittings, we propose to constrain the bulk modulus and its pressure derivative to $K_0 = 162$ GPa and $K_0' = 4.0$–4.5 for uvarovite. Present results were also compared with previous studies for other ugrandite garnets, grossular and andradite, which indicated that the compression mechanism of uvarovite might be similar with grossular and andradite. Furthermore, a systematic relationship, K_0 (GPa) = 398.1(7)–0.136(8) V_0 (Å^3) with a correlation coefficient R^2 of 0.9999, has been established based on these isostructural analogs. Combining these results with previous studies for pyralspite garnets—pyrope, almandine, and spessartine—the compositional dependence of the thermoelastic parameters (bulk modulus, thermal expansion, and the temperature derivative of the bulk modulus) were discussed.

Keywords: Uvarovite, equation of state, high pressure and high temperature, X-ray diffraction, diamond-anvil cell

Introduction

Silicate garnets are considered important rock-forming minerals of the Earth's interior existing in the upper mantle and transition zone, comprising up to 40% by volume of the pyrolite composition and up to 70% of eclogitic composition (Akaogi and Akimoto 1977; Anderson and Bass 1984; Irifune and Ringwood 1987; Ita and Stixrude 1992; Dymshits et al. 2014). They occur as stable phases in a wide range of pressures, temperatures, and chemical environments, and play a fundamental role in high-pressure and high-temperature petrogenetic processes (Deer et al. 1992; Pavese et al. 2001). Garnets are also important components of subducted oceanic crust, and it is suggested that garnet-rich subducted crust can be gravitationally trapped in the lowermost part of transition zone (Irifune and Ringwood 1993; Karato et al. 1995). In addition, former experiments at high pressure and high temperature on garnets showed that post-garnet transitions occur at pressure and temperature conditions relatively close to the ones of the 660 km depth discontinuity (Irifune et al. 1996; Akaogi et al. 1998; Gréaux et al. 2011a, 2011b). Therefore, understanding the thermoelastic properties of garnets is essential to infer appropriate compositional models and regional seismic profiles of the Earth's interior (Duffy and Anderson 1989; Weidner and Wang 2000).

The minerals of the garnet group are divided into two series, pyralspite and ugrandite. Uvarovite is a chromium-bearing ugrandite garnet group species with the formula $Ca_3Cr_2Si_3O_{12}$ and is thus distinguished from both grossularite ($Ca_3Al_2Si_3O_{12}$) and andradite ($Ca_3Fe_2Si_3O_{12}$). Uvarovite is one of the rarest of the garnet group minerals, but nonetheless prevalent in many terrains and geologic settings (Green and Falloon 1998; O'Neill and Palme 1998; Chopelas 2005; Klemme et al. 2005), and its thermoelastic behavior at high pressure and high temperature will shed light on other ugrandite garnets, as well as pyralspite garnets. It can form a complete solid-solution series with grossular and andradite in the Earth's interior (Huckenholz and Knittel 1975). Uvarovite has generally been found associated with serpentinite, chromite, metamorphic limestones, and skarn ore-bodies; it has formed from contact metamorphic processes or hydrothermal processes (Challis et al. 1995; Graham et al. 1996; Proenza et

* Present address: Center for High Pressure Science and Technology Advanced Research, 2699 Qianjin Rd, Changchun, Jilin, 130012, P.R. China. E-mail: fandawei@vip.gyig.ac.cn

al. 1999). In addition, as the Earth's mantle usually contains much more Cr than the Earth's crust (Green and Falloon 1998; O'Neill and Palme 1998), uvarovite is also an important mineral end-member component of most mantle garnets (Klemme et al. 2005). However, it is still among the least investigated garnets in the previous studies. In particular, experimental determinations on the thermoelatic and thermodynamic properties of uvarovite at high-pressure/high-temperature conditions are few (Klemme et al. 2005). Most previous experimental studies focused on the elasticity of uvarovite at high pressure and room temperature (Bass 1986; Leger et al. 1990; Wang and Ji 2001; Diella et al. 2004). Leger et al. (1990) measured the *P-V* equation of state of synthetic uvarovite at high pressure using a diamond-anvil cell instrument with synchrotron radiation X-ray diffraction. Afterward, Diella et al. (2004) examined the elastic parameters of natural uvarovite garnet at high pressure by synchrotron radiation X-ray diffraction by means of a diamond-anvil cell.

To date, the thermoelastic properties of garnets including grossular and andradite have been extensively studied using both the multi-anvil apparatus and the diamond-anvil cell (Gréaux and Yamada 2014; Zou et al. 2012; Gréaux et al. 2011a, 2011b; Fan et al. 2009; Gwanmesia et al. 2006, 2009; Nishihara et al. 2005; Pavese et al. 2001; Wang et al. 1998; Yagi et al. 1987). However, up to now, all of the studies on uvarovite have been limited to either at high pressure and room temperature or at high temperature and ambient pressure. There are no reports in the literature about the thermoelasticity of uvarovite at simultaneously high pressure and high temperature. Therefore, in this study, we have investigated the *P-V-T* relations of a synthetic end-member uvarovite garnet at high pressure and high temperature, using a diamond-anvil cell combined with in situ synchrotron radiation angle-dispersive X-ray diffraction. The thermoelastic property of uvarovite garnet was obtained by the fitting of the present *P-V-T* data to the high-temperature Birch-Murnaghan (HTBM) EoS and thermal pressure EoS. Our results were also discussed with respect to previous reports of thermoelastic properties of other silicate garnets.

Sample and experiment

The uvarovite sample was synthesized using a multi-anvil pressure apparatus (YJ-3000T), at the Institute of Geochemistry, Chinese Academy of Sciences, Guiyang, China. Details of this experimental setup have been described elsewhere by Xie et al. (1993). The pressurization system of this press consists of six WC anvils, with their tips truncated as 23.5 × 23.5 mm^2, which are simultaneously pushed by six hydraulic rams so that high pressure is generated in the experimental assembly (Fan et al. 2013). The pressure in the sample chamber was calibrated by using quartz-coesite phase transition and the high-pressure melting curve of copper, with the error involved in pressure measurement being less than 1.5%. The temperature in the sample chamber was calibrated by means of Pt-$Pt_{90}Rh_{10}$ thermocouple, with the error involved in temperature measurement being less than 5 K (Xie et al. 1993, 2002). The starting materials used in the synthesizing experiments were stoichiometric amounts of high purity calcium carbonate ($CaCO_3$), chromium oxide (Cr_2O_3), aluminum oxide (Al_2O_3), and silica (SiO_2). These mixtures were pretreated at 1200 K in a platinum dish for 12 h to decarbonate. The mixture was then melted at 1700 K, which produced, after quenching, a homogeneous glass. The homogeneous glass was crushed into a fine powder using acetone and then encapsulated in platinum tubes. The synthesizing conditions were 2.5 GPa, 1400 K, and 24 h to form a single phase. The ambient X-ray diffraction data were collected using a D/Max-2200 X-ray diffractometer with graphite crystal monochromator and Cu$K\alpha$ radiation. The ambient X-ray spectrum of uvarovite was indexed according to the standard spectra (JCPDS 82-1914), confirming that the structure of the synthetic uvarovite is cubic, and belongs to the *Ia3d* space group. Its composition was confirmed by using electron microprobe analysis (EPMA-1600).

High-pressure and high-temperature experiments were carried out by using a modified Merrill-Bassett type diamond-anvil cell (DAC). A pair of 500 μm culet-size diamond anvil was used. Gaskets made from stainless steel foil (type T301), pre-indented to a thickness of ~50 μm and then drilled to a diameter of 200 μm, served as the sample chamber. The uvarovite sample powders were slightly pressed between two opposing diamond anvils to form an approximately 25 μm thick disk, and a piece of uvarovite sample about 100 μm in diameter was loaded into the sample chamber. The cell pressure was determined using the equation of state of gold (pressure marker). The pressure transmitting medium was a 16:3:1 mixture ethanol-methanol-water. Heating was carried out by using a resistance-heating system, and the temperature was measured by a $Pt_{90}Rh_{10}$-Pt_{100} thermocouple, which was attached to the pavilion of the diamond.

Figure 1 shows the pressure-temperature (*P-T*) path of the present high-pressure and high-temperature experiments, up to 16 GPa and 900 K. We first compressed the sample up to 10 GPa and then increased the temperature up to 900 K. Heating was maintained at 900 K for several minutes to minimize the effect of non-hydrostatic stress that could develop upon cold compression. Each in situ X-ray diffraction patterns was collected after heating, during cooling down to 300 K, by 200 K steps. Subsequently, the pressure was decreased to ~5 GPa at room temperature. This experimental procedure was repeated for cycles 1 → 6 at the pressure-temperature conditions up to 16 GPa and 900 K. The spectrums were selected after the experiment temperature was kept for ~600 s. Typical exposure times for collecting diffraction patterns of the sample and the pressure marker were 600 s. Details of the experimental setup and cell assembly were described in Fan et al. (2010).

In situ high-pressure and high-temperature angle-dispersive X-ray diffraction experiments were conducted at the 4W2 beamline of the Beijing Synchrotron Radiation Facility (BSRF). An image plate detector (MAR-345) was used to collect diffraction patterns. The wavelength of the monochromatic X-ray beam was 0.6199 Å calibrated by scanning through the Mo metal *K*-absorption edge. The X-ray beam was focused to a beam size of 20 × 30 μm^2 full-width at half maximum (FWHM) by a pair of Kirkpatrick-Baez mirrors. The tilting and rotation of the detector relative to the incident X-ray beam were calibrated using cerium dioxide (CeO_2) powder as the X-ray diffraction standard. The sample-detector distance was calculated from the powder CeO_2 diffraction pattern at ambient conditions. The diffraction patterns were integrated to generate the conventional one-dimensional profiles using the Fit2D program (Hammersley et al. 1996). Analyses of all the patterns were carried out by means of the full profile-fitting technique implemented in the EXPGUI/GSAS software package (Larson and Von Dreele 2000; Toby 2001). Refinement of peak positions and extraction of cell parameters were achieved by reducing full diffraction patterns following the Le Bail method (Le Bail et al. 1988). Precision upon the volume for uvarovite was estimated from the full spectrum fitting (Le Bail refinement) of X-ray diffraction profiles. X-ray diffraction patterns for the uvarovite sample collected at the present experiment pressure and temperature

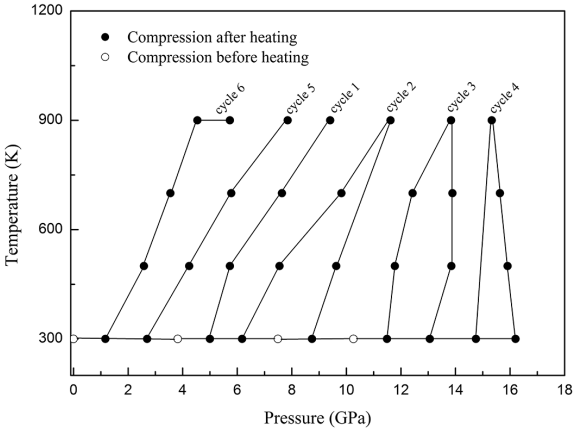

Figure 1. Experimental *P-T* conditions for angle-dispersive synchrotron X-ray diffraction of uvarovite garnet. The solid circle symbols represent the pressures after heating, while open circle symbols show those before heating.

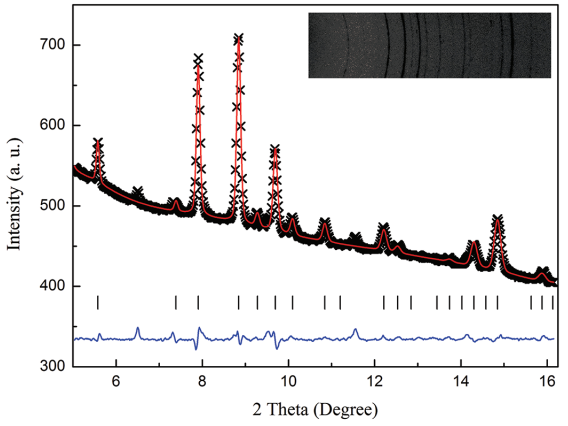

FIGURE 2. Le Bail profile fitting of the diffraction profiles at 15.33 GPa and 900 K of uvarovite. Observed spectra (black line), fitted spectra (red solid line), difference plot (blue solid line), and Bragg peak positions (tick marks) are shown. Inset shows the two-dimensional image of X-ray pattern before the integration of uvarovite at 15.33 GPa and 900 K. (Color online).

conditions showed that no phase transformation were observed throughout these experiments. Figure 2 shows a typical fitting of the full X-ray diffraction pattern at 15.33 GPa and 900 K for uvarovite.

RESULTS AND DISCUSSION

Unit-cell volumes of uvarovite at various pressures and temperatures conditions are shown in Table 1. The results of conventional X-ray diffraction collected at ambient condition gives the unit-cell volume $V_0 = 1736.94 \pm 0.54$ Å^3 for uvarovite in this study, which is in good agreement with the results reported by Carda et al. (1994) (i.e., $V_0 = 1736.87$ Å^3). To derive thermoelastic parameters from the measured *P-V-T* data, we first fitted the compression *P-V* data at the 300 K isotherm to the Birch-Murnaghan equation of state (EoS), and then applied other commonly employed methods, the high-temperature Birch-Murnaghan (HTBM) EoS and thermal pressure EoS approach.

Pressure-volume data at room temperature

Birch-Murnaghan equation of state. The pressure-volume (*P-V*) relations have been determined by fitting the present room-temperature data to a third-order Birch-Murnaghan (III-BM) EoS, which is represented as follows:

$$P = (3/2)K_0[(V_0/V)^{7/3} - (V_0/V)^{5/3}] \times \{1 + (3/4)(K_0' - 4)[(V_0/V)^{2/3} - 1]\} \quad (1)$$

where V_0, K_0, and K_0' are the unit-cell volume, isothermal bulk modulus, and its pressure derivative at ambient condition, respectively. Analyses of Equation 1 with all parameters free yield $V_0 = 1736.9 \pm 0.5$ Å^3, $K_0 = 162 \pm 2$ GPa, $K_0' = 4.5 \pm 0.3$ for uvarovite. With K_0' fixed at 4, the fitting results yield $V_0 = 1736.5 \pm 0.3$ Å^3 and $K_0 = 164 \pm 1$ GPa, respectively. Figure 3 shows the volume compression (V/V_0) of uvarovite as a function of pressure (P) and derived equation of state, and compared with the previous study by Diella et al. (2004).

We used a methanol-ethanol-water mixture with 16:3:1 for the pressure medium in this study, which freezes above 10 GPa, and the hydrostatic circumstance of sample chamber will be influenced. However, the sample chamber in this study has been heated up to 900 K at pressure higher than 10 GPa for the relaxation of the deviatoric stress. Although the effect of deviatoric stress on the unit-cell volume measurements should be small, we still need to assess the impact of non-hydrostatic compression to bulk modulus in this study. In this study, the bulk modulus and its pressure derivative obtained from the hydrostatic conditions (up to 10 GPa, room temperature), $K_0 = 162 \pm 3$ GPa, $K_0' = 4.4 \pm 0.5$, which is very consistent with the results of fitting all the room-temperature data that lead to $K_0 = 162 \pm 2$ GPa, $K_0' = 4.5 \pm 0.3$.

Figure 4 shows the volume Eulerian finite strain ($f_E = [(V_0/V)^{2/3} - 1]$) vs. "normalized pressure" $\{F_E = P/[3f_E(2f_E + 1)^{5/2}]\}$ plot [F_E-f_E plot, (Angel 2000)] of uvarovite in this study. The weighted linear regression through the data points yields the intercept value, $F_E(0) = 162(2)$ GPa for uvarovite,

TABLE 1. Unit-cell parameters of uvarovite at various *P-T* conditions

P^a (GPa)	T (K)	V (Å^3)	P (GPa)	T (K)	V (Å^3)
Compression before heating			9.63(43)	500	1652.58(63)
0.0	300	1736.94(54)	11.78(44)	500	1636.65(45)
3.82(55)	300	1698.55(46)	13.85(67)	500	1619.62(58)
7.49(44)	300	1665.80(76)	15.91(37)	500	1605.23(75)
10.26(48)	300	1642.42(72)	3.55(54)	700	1716.25(66)
Compression after heating			5.78(72)	700	1697.77(38)
1.17(13)	300	1724.71(58)	7.64(49)	700	1679.27(46)
2.70(42)	300	1709.10(22)	9.82(58)	700	1659.47(52)
5.00(34)	300	1686.74(45)	12.43(66)	700	1638.15(61)
6.18(25)	300	1676.44(34)	13.89(69)	700	1624.75(46)
8.74(53)	300	1654.34(54)	15.63(72)	700	1614.55(39)
11.49(63)	300	1631.99(77)	4.54(62)	900	1715.27(84)
13.06(48)	300	1619.53(64)	5.73(47)	900	1705.54(47)
14.75(46)	300	1607.71(58)	7.85(46)	900	1682.69(53)
16.20(31)	300	1598.37(45)	9.41(58)	900	1670.45(54)
2.58(43)	500	1718.38(62)	11.62(47)	900	1652.56(57)
4.24(54)	500	1701.54(36)	13.84(55)	900	1632.62(43)
5.73(58)	500	1690.48(53)	15.33(77)	900	1621.43(48)
7.55(45)	500	1671.43(54)			

Note: Numbers in parentheses represent standard deviations.
[a] Pressure is based on EoS of Au by Fei et al. (2007).

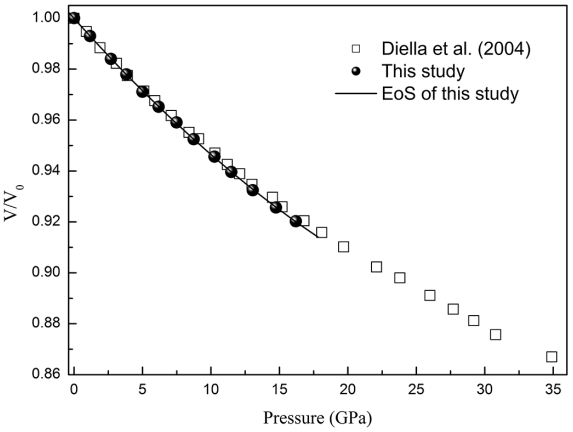

FIGURE 3. Volume compression of uvarovite at high pressure and room temperature in this study compared with the previous study by Diella et al. (2004). The third-order Birch-Murnaghan equation of state fitted with K_0 and K_0' are 162 GPa and 4.5 for uvarovite in this study. The error bars of the data points are smaller than the symbols.

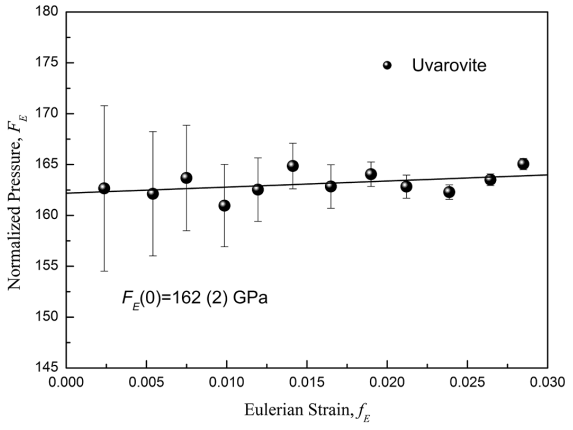

FIGURE 4. Volume Eulerian strain-normalized pressure (F_E-f_E) plot of uvarovite. The solid lines represent the linear fit through the data.

TABLE 2. Bulk modulus and its pressure derivative of ugrandite garnets

Sample	K_0(GPa)	K'_0	V_0 (Å^3)	Methods	Reference
Synthetic Uva	164(1)	4.0[a]	1736.5(3)	XRD	This study (Au-F)[b]
Synthetic Uva	162(2)	4.5(3)	1736.9(5)	XRD	This study (Au-F)
Synthetic Uva	162(2)	—	—	Brillouin	Bass (1986)
Synthetic Uva	162[a]	4.7(7)	—	XRD	Leger et al. (1990)
Natural Uva	164.8(2)	4.7(9)	—	Ultrasonic	Wang and Ji (2001)
Natural Uva	160(1)	5.8(1)	1697.5[a]	XRD	Diella et al. (2004)
Natural Grs	170(4)	5.2(6)	1660.2(3)	XRD	Zhang et al. (1999)
Natural Grs	167.4(2.4)	6.2(5)	1666.4(4)	XRD	Pavese et al. (2001)
Synthetic Grs	171.5(8)	4.42(7)	—	Ultrasonic	Kono et al. (2010)
Synthetic Grs	166(3)	4.0[a]	1664(2)	XRD	Gréaux et al. (2011a)
Synthetic Grs	172(2)	3.0(7)	1664[a]	XRD	Gréaux et al. (2011a)
Natural And	157(2)	4.0[a]	—	Brillouin	Bass (1986)
Synthetic And	162(5)	4.4(7)	—	XRD	Zhang et al. (1999)
Natural And	159.8(2.5)	1.89(1.72)	1754.12(53)	XRD	Pavese et al. (2001)
Natural And	158.5(2.4)	4.0[a]	1753.91(51)	XRD	Pavese et al. (2001)

Notes: XRD = X-ray diffraction; Uva = Uvarovite; Grs = Grossular; And = Andradite. Numbers in parentheses represent standard deviations.
[a] Fixed during fitting.
[b] Pressure was calculated from the equation of state of gold by Fei et al. (2007) (Au-F).

which shows an excellent agreement with the isothermal bulk modulus obtained by the III-BM-EoS. Furthermore, it is clear from Figure 4 that the normalized pressure as a function of the Eulerian strain at 300 K has a positive slope, which is consistent with a value of K'_0 slightly larger than 4 (Angel 2000), showing that the III-BM-EoS is a reasonable description of the *P-V* data in this study.

Vinet equation of state. We also analyzed the *P-V* data using the Vinet EoS (Vinet et al. 1986, 1987). The Vinet EoS was derived from an "universal equation" for solids and results in

$$P(V) = 3K_0 y^{-2}(1-y)\exp[\eta_0(1-y)] \quad (2)$$

where $y = x^{1/3}$, $x = V/V_0$, and $\eta_0 = (3/2)(K'_0 - 1)$. Analyses of Equation 2 with all parameters free yield V_0 = 1736.9 ± 0.6 Å^3, K_0 = 161 ± 3 GPa, K'_0 = 4.4 ± 0.3 for uvarovite, which are reasonably consistent with those derived by the fitting to BM EoS, given V_0 = 1736.9 ± 0.5 Å^3, K_0 = 162 ± 2 GPa, K'_0 = 4.5 ± 0.3 (Table 2). In addition, with K'_0 fixed at 4, the fitting results yield V_0 = 1736.4 ± 0.4 Å^3 and K_0 = 164 ± 1 GPa, respectively, which are also extremely consistent with the results of BM EoS, given V_0 = 1736.5 ± 0.3 Å^3 and K_0 = 164 ± 1 GPa, respectively.

Pressure-volume-temperature data and thermoelastic parameters

High-temperature Birch-Murnaghan equation of state. The *P-V-T* data (Table 1) were used to determine the thermoelastic properties of uvarovite up to ~16 GPa and 900 K. The third-order *P-V-T* Birch-Murnaghan equation of state was applied to our high-pressure and high-temperature data in the form as follows:

$$P = (3/2)\,K_{T0}[(V_{T0}/V)^{7/3} - (V_{T0}/V)^{5/3}] \times \{1 + (3/4)(K'_{T0} - 4)[(V_{T0}/V)^{2/3} - 1]\}. \quad (3)$$

In this equation, the thermal dependences of the zero-pressure volume V_{T0} and bulk modulus K_{T0} at different isotherms are expressed using the following equations

$$V_{T0} = V_0 \exp\int_{300}^{T} \alpha_T dT \quad (4)$$

$$K_{T0} = K_0 + (\partial K_{T0}/\partial T)_P \times (T - 300) \quad (5)$$

where V_0 is the volume at room pressure and temperature, and the temperature derivative for the unit-cell volume V_{T0} can be estimated by a function of the thermal expansion at ambient pressure α_T (Eq. 4). The thermal dependence of the bulk modulus K_{T0} is expressed by a linear function of temperatures, temperature derivative $(\partial K_{T0}/\partial T)_P$ and K_0 (Eq. 5).

The thermoelastic parameters α_T, $(\partial K_T/\partial T)_P$, K_0, and K'_0 obtained for uvarovite in this study are showed in Table 3. Fitting of the present *P-V-T* data to the HTBM EoS yields: V_0 = 1736.8 ± 0.8 Å^3, K_0 = 162 ± 3 GPa, K'_0 = 4.3 ± 0.4, $(\partial K/\partial T)_P$ = –0.021 ± 0.004 GPa/K, and $\alpha_0 = (2.72 \pm 0.14)\times10^{-5}$ K^{-1}. With K'_0 fixed at 4, the fitting results yield V_0 = 1736.6 ± 0.6 Å^3, K_0 = 164 ± 1 GPa, $(\partial K/\partial T)_P$ = –0.018 ± 0.004 GPa/K, and $\alpha_0 = (2.69 \pm 0.12)\times10^{-5}$ K^{-1}, respectively. We also fixed K'_0 to 4.5, which given by *P-V* data in this study, and obtained V_0 = 1737.0 ± 0.6 Å^3, K_0 = 161 ± 1 GPa, $(\partial K/\partial T)_P$ = –0.022 ± 0.004 GPa/K, and $\alpha_0 = (2.76 \pm 0.13)\times10^{-5}$ K^{-1}, respectively. The bulk modulus K_0 and K'_0 determined here are within uncertainties, consistent with the values derived from fitting of our *P-V* data at 300 K. The values of $(\partial K_T/\partial T)_P$ and V_0 within uncertainties are almost unaffected by the choice of K'_0. In addition, the α_0 becomes larger with increasing K'_0 but the difference fall within uncertainties. However, the K_0 slightly deviate because of the strong correlation between K_0 and K'_0. These are very similar to the experimental results of Gréaux and Yamada (2014) for spessartine, and Zou et al. (2012) and Lu et al. (2013) for pyrope, which also showed that the thermal parameter $(\partial K_T/\partial T)_P$ was almost unaffected by the variations of K'_0, whereas the value of K_0 deviate significantly because of the strong correlation between K_0 and K'_0. The measured cell volumes are plotted in Figure 5 as a function of pressure together with the isotherms calculated using the thermoelastic parameters derived from the current fits, showing a good agreement between the fit and the measured *P-V-T* data.

TABLE 3. Thermoelastic parameters of uvarovite compared with other silicate garnets

Sample	V_0 (Å^3)	K_0 (GPa)	K_0'	$(\partial K/\partial T)_P$ (GPa K^{-1})	α_0 (10^{-5}K^{-1})	Reference
Natural Grs	1666.08[a]	168.2(1.7)	4.0[a]	–0.016(3)	2.78(2)	Pavese et al. (2001)
Synthetic Grs	1663.0(10)	159.7(4.0)	5.10(48)	–0.021(2)	2.77(24)	Gréaux et al. (2011a)
Synthetic Grs	1664[a]	166[a]	4.03(13)	–0.019(1)	2.62(23)	Gréaux et al. (2011a)
Natural And	1754.05[a]	158.0(1.5)	4.0[a]	–0.020(3)	3.16(2)	Pavese et al. (2001)
Synthetic Py	1500.7(19)	164(9)	4.9(12)	–0.024(13)	2.97(45)	Zou et al. (2012)
Synthetic Py	1503.1(5)	170(2)	5.0[a]	–0.020(3)	2.30(20)	Wang et al. (1998)
Natural Py	1522.5(8)	167.0(1.8)	4.0(1)	–0.023(2)	–	Lu et al. (2013)
Natural Alm	1539.6(9)	177(2)	4.0[a]	–0.032(16)	3.10(70)	Fan et al. (2009)
$Spe_{38}Alm_{62}$	1544.6(6)	180(4)	4.0(4)	–0.028(5)	3.16(14)	Fan et al. (2015)
$Spe_{64}Alm_{36}$	1557.7(9)	176(4)	4.0(5)	–0.029(5)	3.04(16)	Fan et al. (2015)
Synthetic Spe	1564.96[a]	171(4)	5.3(8)	–0.049(7)	2.46(54)	Gréaux and Yamada (2014)
Synthetic Uva	1736.6(6)	164(1)	4.0[a]	–0.018(4)	2.69(12)	This study (Au-F)[b]
Synthetic Uva	1737.0(6)	161(1)	4.5[a]	–0.022(4)	2.76(13)	This study (Au-F)
Synthetic Uva	1736.8(8)	162(3)	4.3(4)	–0.021(4)	2.72(14)	This study (Au-F)
Synthetic Uva	1736.7(6)	164(1)	4.0[a]	–0.019(4)	2.60(13)	This study (Au-D)
Synthetic Uva	1736.8(8)	163(3)	4.1(3)	–0.020(3)	2.61(14)	This study (Au-D)

Notes: Uva = uvarovite; Grs = grossular; And = andradite; Py = pyrope; Alm = almandine; Spe = spessartine. Numbers in parentheses represent standard deviations.
[a] Fixed during fitting.
[b] Pressure was calculated from the equation of state of gold by Fei et al. (2007) (Au-F) and Dorogokupets and Dewaele (2007) (Au-D).

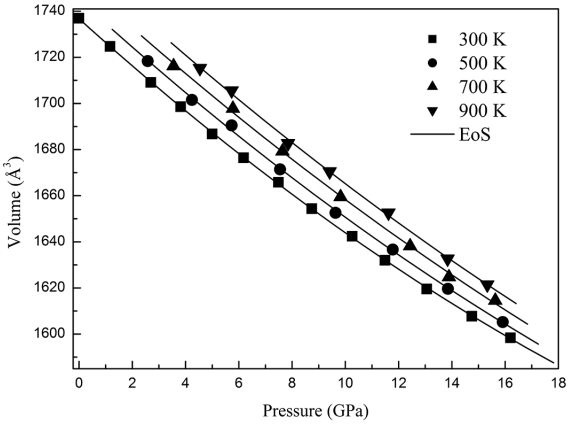

FIGURE 5. Unit-cell volume of uvarovite as a function of pressure and temperature. The solid lines represent isothermal compression curve from fitting HTBM EoS at 300, 500, 700, and 900 K with the following parameters: $K_0 = 162 \pm 3$ GPa, $K_0' = 4.3 \pm 0.4$, $(\partial K/\partial T)_P = -0.021 \pm 0.004$ GPa/K, and $\alpha_0 = (2.72 \pm 0.14)\times10^{-5}$ K^{-1}. The error bars of the data points are smaller than the symbols.

Likewise, we also need to assess the impact of non-hydrostatic compression to thermoelastic parameters in this study. Fitting of the *P-V-T* data at pressures below ~10 GPa to the HTBM EoS yields: $V_0 = 1736.4 \pm 0.9$ Å^3, $K_0 = 164 \pm 4$ GPa, $K_0' = 3.9 \pm 0.6$, $(\partial K/\partial T)_P = -0.020 \pm 0.006$ GPa/K, and $\alpha_0 = (2.65 \pm 0.22)\times10^{-5}$ K^{-1}. With K_0' fixed at 4, the fitting results yield $V_0 = 1736.8 \pm 0.7$ Å^3, $K_0 = 163 \pm 2$ GPa, $(\partial K/\partial T)_P = -0.018 \pm 0.006$ GPa/K, and $\alpha_0 = (2.68 \pm 0.17)\times10^{-5}$ K^{-1}, respectively. These values are very consistent with the results of fitting all the *P-V-T* data that lead to $V_0 = 1736.8 \pm 0.8$ Å^3, $K_0 = 162 \pm 3$ GPa, $K_0' = 4.3 \pm 0.4$, $(\partial K/\partial T)_P = -0.021 \pm 0.004$ GPa/K, and $\alpha_0 = (2.72 \pm 0.14)\times10^{-5}$ K^{-1}. This also indicates that the impact of non-hydrostatic compression to thermoelastic parameters is very limited in this study.

As discussed by some authors (Funamori et al. 1996; Nishihara et al. 2004; Trots et al. 2013; Zhuravlev et al. 2013), the choice of pressure scale maybe affects the thermoelastic parameters derived from *P-V-T* experiments. The pressure scale of Au by Fei et al. (2007) is based on the measured thermoelastic properties of Au at high pressure and high temperature, while the Au pressure scale by Dorogokupets and Dewaele (2007) is based on the expanded Mie-Grüneisen-Debye approach. We also calculated the thermoelastic parameters of uvarovite by using pressure values based on Dorogokupets and Dewaele (2007) (given in Table 3). The value of α_0 is a little bit lowered from 2.69×10^{-5} K^{-1} for Fei et al. (2007) scale to 2.60×10^{-5} K^{-1} using Dorogokupets and Dewaele (2007) scale for $K_0' = 4.0$, while the other parameters are relatively unaffected by the change of scale.

Thermal pressure equation of state. We also analyzed the *P-V-T* data using the thermal pressure approach (e.g., Anderson 1995, 1999; Jackson and Rigden 1996). The thermal pressure ΔP_{th} was obtained by subtracting the pressure at volume V and at room temperature (derived from Eq. 1) from the pressure measured at the same V and at temperature T.

$$\Delta P_{th} = P(V,T) - P(V,300) = \left[\alpha K_T + \left(\frac{\partial K_T}{\partial T}\right)_V \ln\left(\frac{V_0}{V}\right)\right]\times(T-300) \quad (6)$$

Figures 6 and 7 show thermal pressure of uvarovite against temperature and unit-cell volume, respectively. It is seen that thermal pressure of uvarovite varies linearly with temperature and almost independent of volume. A fit of the data in this study yields $K_0 = 162 \pm 2$ GPa, $K_0' = 4.5 \pm 0.6$, and $\alpha_0 = (2.68 \pm 0.18)\times10^{-5}$ K^{-1}, which are reasonably consistent with those derived by the fitting to HTBM EoS (Table 3). Within the uncertainty of the fit $(\partial K_T/\partial T)_V$ value is roughly zero, indicating that the thermal pressure is independent of volume, which is the same with the conclusions of Wang et al. (1998) who also found that the thermal pressure in garnet shows linear variation with T up to 1200 K independent of compression (V/V_0), concluding that $(\partial K_T/\partial T)_V$ is very close to zero. The same conclusions have been drawn for some other silicate minerals, such as olivine (Guyot et al. 1996), $CaSiO_3$ perovskite (Wang et al. 1996), and ringwoodite (Nishihara et al. 2004). By using the thermodynamic relation: $(\partial K_T/\partial T)_P = (\partial K_T/\partial T)_V - \alpha K_T K\partial_T$, we can obtain $(\partial K_T/\partial T)_P = -0.020(3)$ GPa/K. This result is also in good agreement with current analysis using HTBM EoS (Table 3).

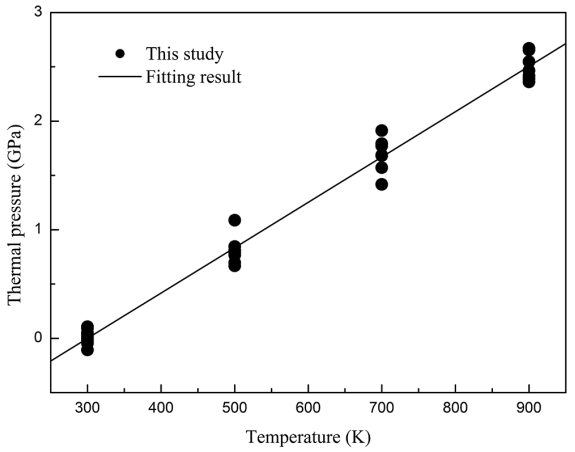

FIGURE 6. Thermal pressure of uvarovite garnet against temperature. Solid circles are uvarovite data in this study. Solid line is the fitting results using thermal pressure approach.

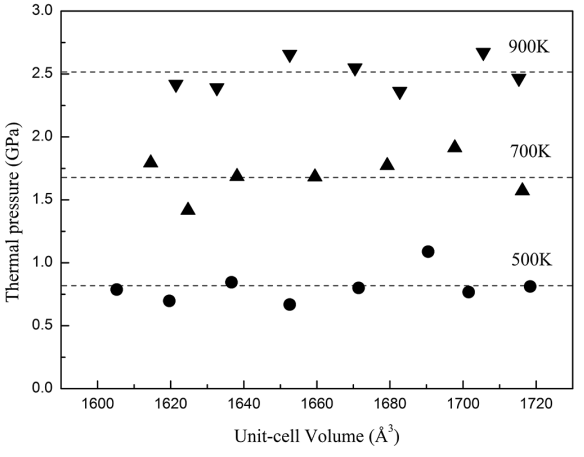

FIGURE 7. Variations of thermal pressure with unit-cell volume at various temperatures. The dash lines correspond to constant values of thermal pressure for a given temperature. The data indicate that $(\partial K_T/\partial T)_V$ is close to zero.

Comparison with other silicate garnets

The current results compared with previous studies for uvarovite are also shown in Table 2. The bulk modulus in this study is in good agreement with previous studies for uvarovite within uncertainties (Bass 1986; Leger et al. 1990; Wang and Ji 2001; Diella et al. 2004). Bass (1986) used Brillouin spectroscopy to study a single crystal of synthetic uvarovite, and reported a very consistent result (K_0 = 162 GPa) with this study. Subsequently, Leger et al. (1990) investigated the behavior of synthetic uvarovite at high pressure and also reported a very similar K_0' of 4.7 with this study (K_0' = 4.7) using the bulk modulus value obtained by Brillouin method (Bass 1986). Wang and Ji (2001) measured the elastic properties of a natural uvarovite by ultrasonic method and given K_0 = 164.8 ± 0.2 GPa, K_0' = 4.7 ± 0.9, which are also very consistent to this study together with Bass (1986) and Leger et al. (1990) within their uncertainties. However, in the case of Diella et al. (2004), their K_0 value of 160 GPa is associated with a higher K_0' of 5.8. As shown in Figure 2, at low pressure our *P-V* relation agrees well with Diella et al. (2004). However, they carried out experiments up to 12 GPa, and then deviations with our data arise above ~12 GPa because of their high K_0' value. Indeed, as shown in Table 2, Diella et al. (2004)'s unit-cell volume is smaller than our study, which is related to their use of natural uvarovite, which contains substantial amounts of Al in the Cr-site. Different techniques employed and sample quality may have influence on the value of K_0' (Huang and Chen 2014). From the comparison of this study with previous results, we propose to constrain the bulk modulus and its pressure derivative to K_0 = 162 GPa and K_0' = 4.0–4.5 for uvarovite.

Another interesting question is how single crystal vs. powder X-ray diffraction methods might influence the elastic/thermoelastic parameters of uvarovite garnet. Rath et al. (2003) investigated the compression behavior of natural uvarovite at high pressure using single-crystal X-ray diffraction and given K_0 = 168 ± 5 GPa. In comparison to the results of powder X-ray diffraction experiments (K_0 = 162 GPa), the bulk modulus of uvarovite from single-crystal X-ray diffraction experiments is a little bit higher than powder X-ray diffraction experiments. However, if consider the uncertainty, they are also consistent each other within their uncertainties. By far, there are not related reports about the thermoelastic properties of uvarovite garnet using single-crystal X-ray diffraction method, what is more, the single-crystal X-ray diffraction experiments of garnet at high pressure and high temperature is also very limited (Lu et al. 2013). But, Lu et al. (2013) measured the single-crystal elasticity of natural Fe-bearing pyrope using in situ Brillouin spectroscopy and X-ray diffraction at simultaneous high *P-T* conditions for the first time, and given the temperature derivative of the bulk modulus for pyrope $(\partial K_T/\partial T)_P$ = –0.023 ± 0.002 GPa/K, which is very consistent to the results from Zou et al. (2012) [$(\partial K_T/\partial T)_P$ = –0.024 ± 0.013 GPa/K] and Wang et al. (1998) [$(\partial K_T/\partial T)_P$ = –0.020 ± 0.003 GPa/K] using powder X-ray diffraction method within their uncertainties. So, there has no important influence on the thermoelastic parameters of pyrope using different X-ray diffraction methods (single crystal vs. powder). In addition, considering the temperature derivative of the bulk modulus for uvarovite is very similar with the results of pyrope (Table 3), we deduce that the influence on the thermoelastic parameters of uvarovite using different X-ray diffraction methods (single crystal vs. powder) maybe also very limited. To confirm it, further examinations through high *P-T* single-crystal X-ray diffraction experiments on the uvarovite garnet are needed.

Elastic properties of other ugrandite garnets-grossular and andradite have been investigated by some authors. Table 2 summarized the bulk moduli and their pressure derivatives for uvarovite together with grossular and andradite determined by various experimental techniques. As shown in Table 2, experimental studies have indicated that the K_0 values of uvarovite from the literatures is about 162 GPa within their uncertainties. However, the K_0 values for andradite and grossular from the literatures exhibit slight discrepancies with each other, ranging from 157 to 162 GPa and 166 to 172 GPa, respectively. From Table 2, we can find that the grossular has the highest incompressibility of the ugrandite garnets; in contrast, the andradite has the lowest incompressibility of the ugrandite garnets, and

the incompressibility of uvarovite is between them. The high-pressure behavior of ugrandite garnets could be explained on the basis of the crystal structure of silicate garnets: The garnet group is composed of minerals of the general formula $X_3Y_2Z_3O_{12}$. The X-site is 8-coordinated (dodecahedra), the Y-site is 6-coordinated (octahedra), and the Z-site is 4-coordinated (tetrahedra). Milman et al. (2001) showed that the bulk modulus of garnet is strongly affected by the bulk modulus of the dodecahedra, but Dymshits et al. (2014) concluded that not only the dodecahedral sites, but also the behavior of the garnet framework and relative sizes of the 8- and 6-coordinated cations, control garnet compression. So, if we compared the effective ionic radius of cations in the octahedral sites of ugrandite garnets cited here, the effective ionic radius of Fe^{3+}(VI) (0.645 Å) for andradite is larger than Cr^{3+}(VI) (0.615 Å) for uvarovite and Al^{3+}(VI) (0.535 Å) for grossular (Shannon 1976). Correspondingly, the mean bond length of Fe^{3+}(VI)-O in andradite (2.019 Å) (Antao 2013) is larger than the mean bond lengths of Cr^{3+}(VI)-O in uvarovite (1.984 Å) (Wildner and Andrut 2001) and Al^{3+}(VI)-O in grossular (1.926 Å) (Geiger and Armbruster 1997). The bond strength of Fe^{3+}(VI)-O in andradite may be weaker than the corresponding bonds in uvarovite and grossular due to the larger bond lengths, accordingly, andradite has a larger compressibility and smaller isothermal bulk modulus (Zhang J. 1999; Milman et al. 2001; Liu X et al. 2008).

Table 2 also lists the available bulk moduli (K_0) and unit-cell volumes (V_0) of the ugrandite garnets, which are important for mantle mineralogy. These K_0-V_0 data are also plotted in Figure 5. The inverse relationship between bulk modulus K_0 and unit-cell volume V_0 has been widely used for predicting bulk moduli of mantle minerals crystallizing in similar structures (Anderson and Anderson 1970; Zhang J. 1999; Liu W et al. 2008; Xiao et al. 2013). It can be expressed as K_0V_0 = constant. To build reliable trends among ugrandite garnets within isostructural groups, it is important to examine the systematic relationships among mantle silicate ugrandite garnets. As can be seen in Figure 8, the three ugrandite garnets exhibit an excellent linear relationship between their unit-cell volumes and bulk moduli. The linear fitting gives a formula as K_0 (GPa) = 398.1(7) – 0.136(8) V_0 (Å^3) with a correlation coefficient R^2 of 0.9999. Obviously, the K_0-V_0 linear function is better than the inverse relationship to predict the bulk modulus of the ugrandite garnets over a wide range of volume and composition. This indicates that there are similar factors governing the compression behaviors in these ugrandite garnets.

The results about the pressure derivative of bulk modulus in this study are also summarized in Table 2 and compared with data for grossular and andradite garnets from previous studies. From the results, we conclude that K_0' for uvarovite garnets from the room-temperature III-BM EoS fit (K_0' = 4.5) and high-temperature III-BM EoS fit (K_0' = 4.3) are entirely identical within the fitting error in this study. They are also very similar to the pressure derivative of bulk modulus for synthetic grossular (K_0' = 4.42) by Kono et al. (2010) and synthetic andradite (K_0' = 4.4) by Zhang et al. (1999). Furthermore, the values of the pressure derivative of bulk modulus for uvarovite garnets in this study are also in excellent agreement with other silicate garnets for which it was proposed that K_0' is close to 4.0 (Zhang et al. 1999; Stixrude and Lithgow-Bertelloni 2005; Gwanmesia et al. 2006; Kono et al. 2010; Gréaux et al. 2011a; Zou et al. 2012; Lu et al. 2013; Huang and Chen 2014). On the other hand, our pressure derivative of K_0' = 4.5(3) cannot agree with that of K_0' = 1.89(1.72) proposed by Pavese et al. (2001) for natural andradite and K_0' = 6.2(5) proposed by Pavese et al. (2001) for natural grossular. Different sample quality may have influence on the determination of K_0' (Huang and Chen 2014). But studies with laser induced phonon spectroscopy (Brillouin scattering) on garnets at high pressures generally result in K_0' ~ 4.0 (Sinogeikin and Bass 2000; Lu et al. 2013; Dymshits et al. 2014), which is considered to be accurate, because it is from direct measurements of elastic moduli at high-pressure conditions (Nishihara et al. 2004, 2005).

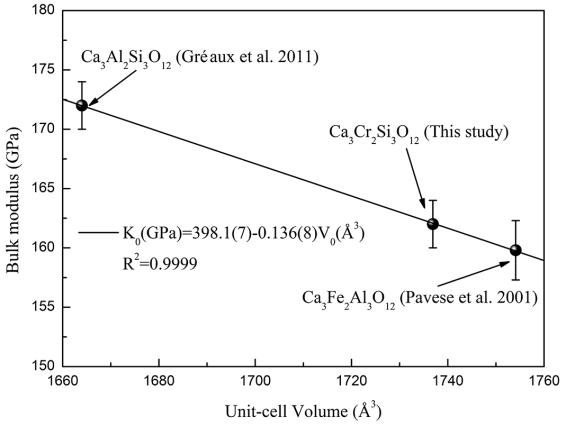

FIGURE 8. The unit formula volume (V_0)–bulk modulus (K_0) relationship of the ugrandite garnets (see Table 2). The K_0-V_0 data of the ugrandite garnets follow an excellent linear function as shown in the plot. The vertical error bars show the estimated standard deviations of the zero-pressure bulk modulus (see Table 2). The uncertainties of the unit formula volume are smaller than the size of the symbols.

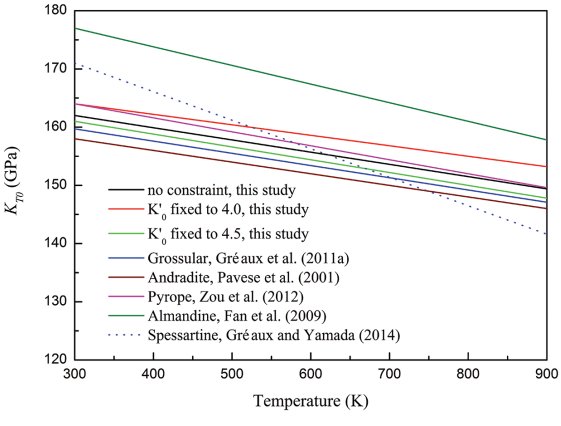

FIGURE 9. Isothermal bulk modulus K_{T0} as a function of temperature. Solid red, green, and black lines represent the present results for fixed values of 4.0 and 4.5, as well as for no constraint on the elastic parameters. Solid blue, wine, magenta, and olive lines and dashed blue lines symbolize the previous studies by Gréaux et al. (2011a) for grossular, Pavese et al. (2001) for andradite, Zou et al. (2012) for pyrope, Fan et al. (2009) for almandine, and Gréaux and Yamada (2014) for spessartine, respectively. (Color online).

Table 3 and Figure 9 show a comparison of the temperature derivative of the bulk modulus for uvarovite in this study to other ugrandite garnets (grossular and andradite), together with pyralspite garnets (pyrope, spessartine, and almandine). It is interesting to note that the temperature derivatives of the bulk modulus in this study for uvarovite at any K_0' are in excellent agreement with each other and other ugrandite garnets, grossular and andradite, within their experimental uncertainties (Table 3 and Fig. 9). Therefore, based on existing data, we believe the temperature derivative of the bulk modulus of ugrandite garnets may not be significant affected by the composition. In addition, the measurement in this study for synthetic uvarovite shows slightly lower the temperature derivative of the bulk modulus than natural almandine by Fan et al. (2009) and natural spessartine-almandine solid solutions ($Spe_{38}Alm_{62}$ and $Spe_{64}Alm_{36}$) by Fan et al. (2015) but the difference fall within uncertainties. What is more, the temperature derivative of the bulk modulus of this study for synthetic uvarovite are also in good agreement with the values of Zou et al. (2012) and Wang et al. (1998) for synthetic pyrope within mutual uncertainties (Table 3). However, the measurements of synthetic spessartine by Gréaux and Yamada (2014) yielded the $(\partial K/\partial T)_P$ values to be –0.049 GPa/K that are obviously higher than all of other silicate garnets. And Figure 9 also shows the variation of bulk modulus with increasing temperature: spessartine softens faster than other silicate garnets. The structural relaxation at high temperature of spessartine may be the reason (Gréaux and Yamada 2014).

Table 3 also summarizes the thermal expansion of uvarovite in this study together with grossular, andradite, and pyralspite garnets—pyrope, spessartine, and almandine. We can also note that the thermal expansion of uvarovite in this study are in good agreement with other ugrandite garnets, grossular and andradite, within their experimental uncertainties (Table 3). In addition, the thermal expansion of synthetic uvarovite in this study are also in excellent agreement with the values of Zou et al. (2012) and Wang et al. (1998) for pyrope, Fan et al. (2009) for almandine, and Gréaux and Yamada (2014) for spessartine within mutual uncertainties (Table 3). In particularly, the thermal expansion for uvarovite in this study is also very consistent with the values of Fan et al. (2015) for spessartine-almandine solid solution within their uncertainties (Table 3). Therefore, based on existing data, we believe the thermal expansion of silicate garnet may not be significant affected by the composition, which is similar with the view of Nishihara et al. (2005) and Fan et al. (2015) who considered that the thermal expansion coefficients on garnets show similar values regardless of the garnet chemistry.

IMPLICATIONS

As experimentally confirmed, garnet occurs commonly in nature both as a metamorphic mineral and as a high-pressure phase, stable under upper mantle conditions (Leitner et al. 1980), and is probably also important in the mantle-transition zone (420–670 km) (Duffy and Anderson 1989). A knowledge of the thermoelastic and thermodynamic properties of garnets is, therefore, of great geophysical importance in the characterization of the thermal structure and phase equilibria, and the construction of the upper mantle and transition zone composition models of the Earth's interior (Duffy and Anderson 1989; Weidner and Wang 2000).

Cr-rich minerals are a common mineral phase in the Earth's mantle and crust (Cookenboo and Grutter 2010; Klemme 2004; Liou et al. 2009; Stachel and Harris 1997; van Roermund 2009). In particular, Cr-rich garnets (knorringite and uvarovite) are commonly found in the deep Earth, as indicated by xenoliths in kimberlites and inclusions in diamonds (e.g., Nixon 1995; Stachel and Harris 1997; Stachel et al. 1998; Bulanova et al. 2004). Furthermore, chromium concentration in garnet increases with depth and is used in mantle barometry (Grüttler et al. 2006). The presence of Cr in the garnet lattice shifts significantly the spinel-garnet transformation—a major phase boundary in the Earth's upper mantle—to pressures as high as 7 GPa (Klemme 2004). Pyrope and knorringite form a complete solid solution and garnets close to the pyrope 50-knorrigite 50 composition occur as inclusions in natural diamonds (Irifune et al. 1982). Therefore, the thermoelastic and thermodynamic properties of Cr-bearing garnets (knorringite and uvarovite) at high pressure and high temperature is essential to evaluate the phase relations and thermal structure of the Earth's mantle. However, to date, meaningful thermal structure and phase relations calculations in realistic mantle compositions cannot be performed, as thermoelastic and thermodynamic data for many Cr-rich minerals (such as knorringite and uvarovite) are not as well understood as one would wish (e.g., Asimov et al. 1995; Klemme 2004). In addition, the high-pressure phase relations and stability of knorringite are controversial (Ringwood 1977; Irifune et al. 1982; Turkin et al. 1983; Klemme 2004; Zou and Irifune 2012). Furthermore, pure knorringite garnet may be not a stable phase under the pressure and temperature conditions of upper mantle and transition zone of deep-Earth (Zou and Irifune 2012), and high-precision thermoelastic and thermodynamic data probably will never be available for this phase. However, our results show that uvarovite is still stable at the present experiment pressure and temperature conditions which are already close to the *P-T* conditions of upper mantle, so our results here may be used as analogs to understanding the thermoelastic and thermodynamic properties of knorringite and Cr-bearing garnets in the deep-Earth mantle. Moreover, the determination of thermoelastic property of uvarovite ($Ca_3Cr_2Si_3O_{12}$) at high-pressure and high-temperature conditions in this study will also shed light on the thermal structure and phase relations of the Earth's mantle. However, detailed knowledges of the high-pressure and high-temperature phase relations and thermodynamic parameters of the Cr-bearing garnets at the *P-T* conditions of the upper mantle and transition zone will be needed to fully explore the thermodynamic stability of the deep-Earth mantle.

Additionally, the experimental study of silicate garnet end-members at high pressure and high temperature is also of great importance to constrain the compositional dependence of thermoelastic properties in those minerals (Gréaux et al. 2011a, 2011b; Zou et al. 2012; Huang and Chen 2014). Such results are particularly valuable for the understanding of natural garnets' behavior at high pressure and high temperature since they usually display relatively complex composition (Gréaux and Yamada 2014). Based on the high-pressure and high-temperature angle-dispersive X-ray diffraction experiments on uvarovite in this study and relevant literature data for grossular and andradite, we

conclude that the compression mechanism of uvarovite might be similar with grossular and andradite. And the three ugrandite garnets exhibit an excellent linear relationship between their unit-cell volumes and bulk moduli [K_0(GPa) = 398.1(7) – 0.136(8) V_0(Å^3), R^2 = 0.9999], which is very important to examine the systematic relationships among mantle silicate ugrandite garnets. On the one hand, the thermoelastic properties of uvarovite at high pressure and high temperature in this study together with other studies for grossular and andradite will provide a direct assessment of thermoelastic behavior of ugrandite garnets at simultaneous high pressure and high temperature (Gréaux et al. 2011a; Pavese et al. 2001). On the other hand, these new data set thus allows us to place improved constraints on the compositional dependence of thermoelastic parameters in the rocks of the upper mantle and transition zone (Jiang et al. 2004; Gwanmesia et al. 2009; Lu et al. 2013). Moreover, considering the abundance of garnets in the Earth's upper mantle and transition zone, experimental studies on the thermoelasticity of garnets with a relevant composition at upper-mantle pressure and temperature conditions have significantly implications for understanding the chemical composition of the deep Earth (Bass and Anderson 1984; Duffy and Anderson 1989; Cammarano et al. 2003; Li and Liebermann 2007), so these data also can be used to contribute to construction of compositional model of Earth's interior (Lu et al. 2013).

Acknowledgments

We thank Associate Editor Haozhe Liu and the anonymous reviewers for the constructive comments and suggestions. This work is supported by the National Natural Science Foundation of China (Grants No. 41374107, 41274105), the youth innovative technology talents program of Institute of Geochemistry, Chinese Academy of Sciences (2013, to Dawei Fan), the western doctor special fund of the West Light Foundation of Chinese Academy of Sciences (2011, to Dawei Fan). The high-pressure X-ray diffraction experiments were taken at the High Pressure Experiment Station (4W2), Beijing Synchrotron Radiation Facility (BSRF).

References cited

Akaogi, M., and Akimoto, S. (1977) Pyroxene-garnet solid-solution equilibria in the systems $Mg_4Si_4O_{12}$-$Mg_3Al_2Si_3O_{12}$ and $Fe_4Si_4O_{12}$-$Fe_3Al_2Si_3O_{12}$ at high pressures and temperatures. Physics of the Earth and Planetary Interiors, 15, 90–106.

Akaogi, M., Ohmura, N., and Suzuki, T. (1998) High-pressure dissociation of $Fe_3Al_2Si_3O_{12}$ garnet: phase boundary determined by phase equilibrium experiments and calorimetry. Physics of the Earth and Planetary Interiors, 106, 103–113.

Anderson, O.L. (1995) equation of state of Solids for Geophysics and Ceramic Science, p. 243–274. Oxford University Press, New York.

Anderson, D.L., and Anderson, O.L. (1970) The bulk modulus-volume relationship for oxides. Journal of Geophysical Research, 75, 3494–3500.

Anderson, D.L., and Bass, J.D. (1984) Mineralogy and composition of the upper mantle. Geophysical Research Letters, 11, 637–640.

Angel, R. (2000) Equation of state. Reviews in Mineralogy and Geochemistry, 41, 35–60.

Antao, S.M. (2013) Three cubic phases intergrown in a birefringent andradite-grossular garnet and their implications. Physics and Chemistry of Minerals, 40, 705–716.

Asimov, P.D., Hirschmann, M.M., Ghiorso, M.S., O'Hara, M.J., and Stolper, E.M. (1995) The effect of pressure induced solid-solid phase transitions on decompression melting of the mantle. Geochimica et Cosmochimica Acta, 59, 4489–4506.

Bass, J.D. (1986) Elasticity of uvarovite and andradite garnets. Journal of Geophysical Research, 91, 7505–7516.

Bass, J.D., and Anderson, D.L. (1984) Composition of the upper mantle: geophysical tests of two petrological models. Geophysical Research Letters, 11, 229–232.

Bulanova, G.P., Muchemwa, E., Pearson, D.G., Griffin, B.J., Kelley, S.P., Klemme, S., and Smith, C.B. (2004) Syngenetic inclusions in diamond from Sesekimberlite (Zimbabwe)-evidence for metasomatic conditions of growth. Lithos, 77, 181–192.

Cammarano, F., Goes, S., Vacher, P., and Giardini, D. (2003) Inferring upper-mantle temperatures from seismic velocities. Physics of the Earth and Planetary Interiors, 138, 197–222.

Challis, A., Grapes, R., and Palmer, K. (1995) Chromian muscovite, uvarovite, and zincian chromite: Products of regional metasomatism in northwest Nelson, New Zealand. Canadian Mineralogist, 33, 1263–1284.

Chopelas, A. (2005) Single crystal Raman spectrum of uvarovite, $Ca_3Cr_2Si_3O_{12}$. Physics and Chemistry of Minerals, 32, 525–530.

Cookenboo, H.O., and Grütter, H.S. (2010) Mantle-derived indicator mineral compositions as applied to diamond exploration. Geochemistry: Exploration, Environment, Analysis, 10, 81–95.

Deer, W.A., Howie, R.A., and Zussman, J. (1992) An Introduction to the Rock-Forming Minerals. Wiley, New York.

Diella, V., Sani, A., Levy, D., and Pavese, A. (2004) High-pressure synchrotron X-ray diffraction study of spessartine and uvarovite: a comparison between different equation of state models. American Mineralogist, 89, 371–376.

Duffy, T.S., and Anderson, D.L. (1989) Seismic velocity in mantle minerals and mineralogy of the upper mantle. Journal of Geophysical Research, 94, 1895–1912.

Dymshits, A.M., Litasov, K.D., Shatskiy, A., Sharygin, I.S., Ohtani, E., Suzuki, A., Pokhilenko, N.P., and Funakoshi, K. (2014) *P-V-T* equation of state of Na-majorite to 21 GPa and 1673 K. Physics of the Earth and Planetary Interiors, 227, 68–75.

Fan, D.W., Zhou, W.G., Liu, C.Q., Liu, Y.G., Wan, F., Xing, Y.S., Liu, J., Bai, L.G., and Xie, H.S. (2009) The thermal equation of state of $(Fe_{0.86}Mg_{0.07}Mn_{0.07})_3Al_2Si_3O_{12}$ almandine. Mineralogical Magazine, 73, 95–102.

Fan, D.W., Zhou, W.G., Wei, S.Y., Liu, Y.G., Ma, M.N., and Xie, H.S. (2010) A simple external resistance heating diamond anvil cell and its application for synchrotron radiation X-ray diffraction. Review of Scientific Instruments, 81, 053903.

Fan, D.W., Ma, M.N., Wei, S.Y., Chen, Z.Q., and Xie, H.S. (2013) High pressure elastic behavior of synthetic $Mg_3Y_2(SiO_4)_3$ garnet up to 9GPa. Advances in Materials Science and Engineering, 2013, 502702.

Fan, D.W., Xu, J.G., Ma, M.N., Wei, S.Y., Liu, J., and Xie, H.S. (2015) *P-V-T* equation of state of spessartine-almandine solid solution measured using a diamond anvil cell and in situ synchrotron X-ray diffraction. Physics and Chemistry of Minerals, 42, 63–72, http://dx.doi.org/10.1007/s00269-014-0700-2.

Fei, Y.W., Ricolleau, A., Frank, M., Mibe, K., Shen, G.Y., and Prakapenka, V. (2007) Toward an internally consistent pressure scale. Proceedings of the National Academy of Sciences, 104, 9182–9186.

Funamori, N., Yagi, T., Utsumi, W., Kondo, T., Uchida, T., Funamori, M. (1996) Simultaneous high-*P*, high-*T* X-ray diffraction study of β-$(Mg, Fe)_2SiO_4$ to 26 GPa and 900 K. Journal of Geophysical Research, 101, 8257–8269.

Geiger, C.A., and Armbruster, T. (1997) $Mn_3Al_2Si_3O_{12}$ spessartine and $Ca_3Al_2Si_3O_{12}$ grossular garnet: Structural dynamic and thermodynamic properties. American Mineralogist, 82, 740–747.

Graham, I.T., Franklin, B.J., and Marshall, B. (1996) Chemistry and mineralogy of podiform chromitite deposits, southern NSW, Australia: A guide to their origin and evolution. Mineralogy and Petrology, 57, 129–150.

Gréaux, S., and Yamada, A. (2014) P-*V-T* equation of state of $Mn_3Al_2Si_3O_{12}$ spessartine garnet. Physics and Chemistry of Minerals, 41, 141–149.

Gréaux, S., Kono, Y., Nishiyama, N., Kunimoto, T., Wada, K., and Irifune, T. (2011a) *P-V-T* equation of state of $Ca_3Al_2Si_3O_{12}$ grossular garnet. Physics and Chemistry of Minerals, 38, 85–94.

Gréaux, S., Nishiyama, N., Kono, Y., Gautron, L., Ohfuji, H., Kunimoto, T., Menguy, N., and Irifune, T. (2011b) Phase transformations of $Ca_3Al_2Si_3O_{12}$ grossular garnet to the depths of the Earth's mantle transition zone. Physics of the Earth and Planetary Interiors, 185, 89–99.

Green, D.H., and Falloon, T.J. (1998) Pyrolite: A ringwood concept and its current expression. In Jackson, I., Ed., The Earth's Mantle: Composition, structure and evolution, p. 311–380. Cambridge University Press, U.K.

Grüttler, H., Latti, D., and Menzies, A. (2006) Cr-saturation in concentrate garnet compositions from kimberlite and their use in mantle barometry. Journal of Petrology, 47, 801–820.

Guyot, F., Wang, Y., Gillet, P., and Ricard, Y. (1996) Quasiharmonic computations of thermodynamic parameters of olivines at high pressure and high temperature: a comparison with experiment data. Physics of the Earth and Planetary Interiors, 98, 17–29.

Gwanmesia, G.D., Zhang, J., Darling, K., Kung, J., Li, B., Wang, L., Neuville, D., and Liebermann, R.C. (2006) Elasticity of polycrystalline pyrope $Mg_3Al_2Si_3O_{12}$ to 9 GPa and 1,000°C. Physics of the Earth and Planetary Interiors, 155, 179–190.

Gwanmesia, G.D., Wang, L., Triplett, R., and Liebermann, R.C. (2009) Pressure and temperature dependence of the elasticity of pyrope-majorite [$Py_{60}Mj_{40}$ and $Py_{50}Mj_{50}$] garnet solid solution measured by ultrasonic interferometry technique. Physics of the Earth and Planetary Interiors, 174, 105–112.

Hammersley, A.P., Svensson, S.O., Hanfland, M., Fitch, A.N., and Hausermann, D. (1996) Two-dimensional detector software: from real detector to idealized image or two-theta scan. High Pressure Research, 14, 235–248.

Huang, S., and Chen, J.H. (2014) Equation of state of pyrope–almandine solid solution measured using a diamond anvil cell and *in situ* synchrotron X-ray diffraction. Physics of the Earth and Planetary Interiors, 228, 88–91.

Huckenholz, H.G., and Knittel, D. (1975) Uvarovite: stability of uvarovite-grossular solid solution at low pressure. Contributions to Mineralogy and Petrology, 49, 211–232.

Irifune, T., and Ringwood, A.E. (1987) Phase transformations in a harzburgite composition to 26 GPa: implications for dynamical behaviour of the subducting

slab. Earth and Planetary Science Letters, 86, 365–376.
——— (1993) Phase transformation in subducted oceanic crust and buoyancy relationships at depths of 600–800 km in the mantle. Earth and Planetary Science Letters, 117, 101–110.
Irifune, T., Ohtani, E., and Kumazawa, M. (1982) Stability field of knorringite $Mg_3Cr_2Si_3O_{12}$ at high pressure and high temperature and its implication to the occurrence of Cr-rich pyrope in upper mantle. Physics of the Earth and Planetary Interiors, 27, 263–272.
Irifune, T., Koizumi, T., and Ando, J. (1996) An experimental study of the garnet-perovskite transformation in the system $MgSiO_3$-$Mg_3Al_2Si_3O_{12}$. Physics of the Earth and Planetary Interiors, 96, 147–157.
Ita, J., and Stixrude, L. (1992) Petrology, elasticity, and composition of the mantle transition zone. Journal of Geophysical Research, 97, 6849–6866.
Jackson, I., and Rigden, S.M. (1996) Analysis of *P-V-T* data: Constraints on the thermoelastic properties of high-pressure minerals. Physics of the Earth and Planetary Interiors, 96, 85–112.
Jiang, F.M., Speziale, S., and Duffy, T.S. (2004) Single-crystal elasticity of grossular- and almandine-rich garnets to 11 GPa by Brillouin scattering. Journal of Geophysical Research, 109, B10210.
Karato, S., Wang, Z., Liu, B., and Fujino, K. (1995) Plastic deformation of garnets: systematics and implications for the rheology of the mantle transition zone. Earth and Planetary Science Letters, 130, 13–30.
Klemme, S. (2004) The influence of Cr on the garnet-spinel transition in the Earth's mantle: Experiments in the system MgO-Cr_2O_3-SiO_2 and thermodynamic modelling. Lithos, 77, 639–646.
Klemme, S., Van Miltenburg, J.C., Javorsky, P., and Wastin, F. (2005) Thermodynamic properties of uvarovite garnet ($Ca_3Cr_2Si_3O_{12}$). American Mineralogist, 90, 663–666.
Kono, Y., Gréaux, S., Higo, Y., Ohfuji, H., and Irifune, T. (2010) Pressure and temperature dependences of elastic properties of grossular garnet up to 17 GPa and 1 650 K. Journal of Earth Science, 21, 782–791.
Larson, A.C., and Von Dreele, R.B. (2000) GSAS, General Structure Analysis System operation manual. Los Alamos National Laboratory LAUR 86-748, 1–179.
Le Bail, A., Duroy, H., and Fourquet, J.L. (1988) Ab initio structure determination of $LiSbWO_6$ by X-ray powder diffraction. Materials Research Bulletin, 23, 447–452.
Leger, J.M., Redon, A.M., and Chateau, C. (1990) Compressions of synthetic pyrope, spessartine and uvarovite garnets up to 25 GPa. Physics and Chemistry of Minerals, 17, 161–167.
Leitner, B.J., Weidner, D.J., and Liebermann, R.C. (1980) Elasticity of single crystal pyrope and implications for garnet solid solution series. Physics of the Earth and Planetary Interiors, 22, 111–121.
Li, B., and Liebermann, R.C. (2007) Indoor seismology by probing the Earth's interior by using sound velocity measurements at high pressures and temperature. Proceedings of the National Academy of Sciences, 104, 9145–9150.
Liou, J.G., Ernst, W.G., Zhang, R.Y., Tsujimori, T., and Jahn, B.M. (2009) Ultrahigh-pressure minerals and metamorphic terranes—The view from China. Journal of Asian Earth Sciences, 35, 199–231.
Liu, W., Kung, J., Wang, L.P., and Li, B.S. (2008) Thermal equation of state of $CaGeO_3$ perovskite. American Mineralogist, 93, 745–750.
Liu, X., Shieh, S.R., Fleet, M.E., and Akhmetov, A. (2008) High-pressure study on lead fluorapatite. American Mineralogist, 93, 1581–1584.
Lu, C., Mao, Z., Lin, J.F., Zhuravlev, K.K., Tkachev, S.N., and Prakapenka, V.B. (2013) Elasticity of single-crystal iron-bearing pyrope up to 20 GPa and 750 K. Earth and Planetary Science Letters, 361, 134–142.
Milman, V., Akhmatskaya, E., Nobes, R., Winkler, B., Pickard, C., and White, J. (2001) Systematic *ab initio* study of the compressibility of silicate garnets. Acta Crystallographica Section B, 57, 163–177.
Nishihara, Y., Takahashi, E., Matsukage, K.N., Iguchi, T., Nakayama, K., and Funakoshi, K. (2004) Thermal equation of state ($Mg_{0.91}Fe_{0.09})_2SiO_4$ ringwoodite. Physics of the Earth and Planetary Interiors, 143-144, 33–46.
Nishihara, Y., Aoki, I., Takahashi, E., Matsukage, K.N., and Funakoshi, K.I. (2005) Thermal equation of state of majorite with MORB composition. Physics of the Earth and Planetary Interiors, 148, 73–84.
Nixon, P.H. (1995) A review of mantle xenoliths and their role in diamond exploration. Journal of Geodynamics, 20, 305–329.
O'Neill, H.St.C., and Palme, H. (1998) Composition of the silicate Earth: Implications for accretion and core formation. In Jackson, I., Ed., The Earth's Mantle: Composition, structure and evolution, p. 3–126. Cambridge University Press, U.K.
Pavese, A., Diella, V., Pischedda, V., Merli, M., Bocchio, R., and Mezouar, M. (2001) Pressure-volume-temperature equation of state of andradite and grossular, by high-pressure and -temperature powder diffraction. Physics and Chemistry of Minerals, 28, 242–248.
Proenza, J., Sole, J., and Melgarejo, J.C. (1999) Uvarovite in podiform chro-mitite: The Moa-Baracoa ophiolitic massif, Cuba. Canadian Mineralogist, 37, 679–690.
Rath, S., Knorr, K., and Morgenroth, W. (2003) High-pressure investigation on single crystal uvarovite, $Ca_3Cr_2Si_3O_{12}$. Hasylab Annual Report, Germany.
Ringwood, A.E. (1977) Synthesis of pyrope-knorringite solid solutions series. Earth and Planetary Science Letters, 36, 443–448.
Shannon, R.D. (1976) Revised effective ionic-radii and systematic studies of interatomic distances in halides and chalcogenides. Acta Crystallographica Section A, 32, 751–767.
Sinogeikin, S.V., and Bass, J.D. (2000) Single-crystal elasticity of pyrope and MgO to 20 GPa by Brillouin scattering in the diamond cell. Physics of the Earth and Planetary Interiors, 120, 43–62.
Stachel, T., and Harris, J.W. (1997) Syngenetic inclusions in diamond from the Birim field (Ghana)—A deep peridotitic profile with a history of depletion and re-enrichment. Contributions to Mineralogy and Petrology, 127, 336–352.
Stachel, T., Viljoen, K.S., Brey, G.P., and Harris, J.W. (1998) Metasomatic processes in lherzolitic and harzburgitic domains of diamondiferous lithospheric mantle-REE in garnets from xenoliths and inclusions in diamonds. Earth and Planetary Science Letters, 159, 1–12.
Stixrude, L., and Lithgow-Bertelloni, C. (2005) Thermodynamics of mantle minerals—I. Physical properties. Geophysical Journal International, 162, 610–632.
Toby, B.H. (2001) EXPGUI, a graphical user interface for GSAS. Journal of Applied Crystallography, 34, 210–213.
Trots, D.M., Kurnosov, A., Ballaran, T.B., Tkachev, S., Zhuravlev, K., Prakapenka, V., Berkowski, M., and Frost, D.J. (2013) The Sm:YAG primary fluorescence pressure scale. Journal of Geophysical Research, 118, 5805–5813.
Turkin, A.I., Doroshev, A.M., and Malinovskii, I.Y. (1983) A study of the phase composition of garnet-bearing assemblages in the system MgO-Al_2O_3-Cr_2O_3-SiO_2 at high temperatures and pressures. In Silicate Systems at High Pressures, 5–24. Institute of Geology and Geophysics, Novosibirsk (in Russian).
van Roermund, H. (2009) Mantle-wedge garnet peridotites from the northernmost ultra-high pressure domain of the Western Gneiss Region, SW Norway. European Journal of Mineralogy, 21, 1085–1096.
Vinet, P., Ferrante, J., Rose, J.H., and Smith, J.R. (1987) Compressibility of solids. Journal of Geophysical Research, 92, 9319–9325.
Vinet, P., Ferrante, J., Smith, J.R., and Rose, J.H. (1986) A universal equation of state for solids. Journal of Physics C: Solid State Physics, 19, L467.
Wang, Y., Weinder, D.J., and Guyot, F. (1996) Thermal equation of state of $CaSiO_3$ perovskite. Journal of Geophysical Research, 101, 661–672.
Wang, Y., Weidner, D.J., Zhang, J., Gwanmesia, G.D., and Liebermann, R.C. (1998) Thermal equation of state of garnets along the pyrope-majorite join. Physics of the Earth and Planetary Interiors, 105, 59–71.
Wang, Z.C., and Ji, S.C. (2001) Elasticity of six polycrystalline silicate garnets at pressure up to 3.0 GPa. American Mineralogist, 86, 1209–1218.
Weidner, D.J., and Wang, Y. (2000) Phase transformations: Implications for mantle structure. Geophysical Monograph Series, 117, 215–235.
Wildner, M., and Andrut, M. (2001) The crystal chemistry of birefringent natural uvarovites: Part II. Single-crystal X-ray structures, American Mineralogist, 86, 1231–1251.
Xiao, W.S., Tan, D.Y., Zhou, W., Liu, J., and Xu, J. (2013) Cubic perovskite polymorph of strontium metasilicate at high pressures. American Mineralogist, 98, 2096–2104.
Xie, H.S., Zhang, Y., Xu, H.G., Hou, W., Guo, J., and Zhao, H. (1993) A new method of measurement for elastic wave velocities in minerals and rocks at high temperature and high pressure and its significance. Science China Chemistry, 36, 1276–1280.
Xie, H.S., Zhou, W.G., Liu, Y.G., Guo, J., Hou, W., and Zhao, Z.D. (2002) Comparative experimental study on several methods for measuring elastic wave velocities in rocks at high pressure. Science China Earth Sciences, 45, 990–998.
Yagi, T., Akaogi, M., Shimomura, O., Tamai, H., and Akimoto, S.I. (1987) High pressure and high temperature equations of state of majorite. Geophysical Monograph Series, 39, 141–147.
Zhang, J. (1999) Room-temperature compressibilities of MnO and CdO: further examination of the role of cation type in bulk modulus systematic. Physics and Chemistry of Minerals, 26, 644–648.
Zhang, L., Ahsbahs, H., Kutoglu, A., and Geiger, C.A. (1999) Single-crystal hydrostatic compression of synthetic pyrope, almandine, spessartine, grossular and andradite garnets at high pressure. Physics and Chemistry of Minerals, 27, 52–58.
Zhuravlev, K.K., Goncharov, A.F., Tkachev, S.N., Dera, P., and Prakapenka, V.B. (2013) Vibrational, elastic, and structural properties of cubic silicon carbide under pressure up to 75 GPa: Implication for a primary pressure scale. Journal of Applied Physics, 113, 113503.
Zou, Y., and Irifune, T. (2012) Phase relations in $Mg_3Cr_2Si_3O_{12}$ and formation of majoritic knorringite garnet at high pressure and high temperature. Journal of Mineralogical and Petrological Sciences, 107, 197–205.
Zou, Y., Gréaux, S., Irifune, T., Whitaker, M.L., Shinmei, T., and Higo, Y. (2012) Thermal equation of state of $Mg_3Al_2Si_3O_{12}$ pyrope garnet up to 19 GPa and 1700 K. Physics and Chemistry of Minerals, 39, 589–598.

Manuscript received April 9, 2014
Manuscript accepted September 20, 2014
Manuscript handled by Haozhe Liu